Optics and Lasers in Engineering 132 (2020) 106134

Contents lists available at ScienceDirect

Optics and Lasers in Engineering

journal homepage: www.elsevier.com/locate/optlaseng

Phase extraction from two randomly phase shifted interferograms by combining advanced principal component analysis and Lissajous ellipse fitting

Yu Zhang [a,b,*], Xiaobo Tian [c], Rongguang Liang [c]

[a] Institute of Materials Physics, College of Science, Northeast Electric Power University, Jilin, Jilin 132012, China
[b] State Key Laboratory of Applied Optics, Changchun Institute of Optics, Fine Mechanics and Physics, Chinese Academy of Sciences, Changchun, Jilin 130022, China
[c] College of Optical Sciences, University of Arizona, Tucson, Arizona 85721, USA

ARTICLE INFO

Keywords:
Phase shifting algorithm
Advanced principal component analysis
Lissajous ellipse fitting
Pre-filtering

ABSTRACT

In order to achieve the high accuracy and high speed in phase shifting interferometry, a phase extraction approach by combining advanced principal component analysis and Lissajous ellipse fitting (APCA-LEF) is proposed. It can obtain accurate phase distribution with only two no pre-filtering phase shifted interferograms, and it costs less time simultaneously. It removes the restriction that PCA needs more than three interferograms with well distributed phase shifts to subtract relatively accurate mean. Moreover, adjacent pixels taken part in the APCA process increases the accuracy by suppressing the effect of noise, also, it is suitable for different levels of noises. Last but not least, if the high accuracy is required, the phase shift would be best to far away from 0 rad and π rad. The simulations and experiments verify the correctness and feasibility of APCA-LEF.

1. Introduction

Phase shifting interferometry (PSI) has been widely used in optical measurement [1–3]. For the fixed interferometer and environment, the performance of PSI mainly depends on the phase shifting algorithm (PSA). Some traditional algorithms, such as 3-step, 4-step, 5-step, and N-step PSAs etc., require the fixed phase shifts [4]. However, it is difficult to obtain the accurate phase shift due to phase shift error caused by the miscalibration of piezo-transducer (PZT), vibrational error, air turbulence, instability of the laser frequency [4–6]. Hence, many random PSAs have been developed to remove the effect of the phase shift error, it can be divided into the iterative and non-iterative PSAs. In general, the iterative PSAs have high accuracy, but they cost more time, and the non-iterative PSAs spend less time than the iterative PSAs, but the accuracy may be not as high as the iterative PSAs. In recent years, in-situ measurement technology has been widely developed, both the accuracy and working time of PSI need to be considered. Because the computational time of the iterative PSAs are difficult to reduce, only a small number of iterative PSAs have been developed [7–9]. Hence, most scientists were committed to research the non-iterative random PSAs with high accuracy.

In 1992, Farrell and Player utilized Lissajous figures and ellipse fitting to calculate the phase difference between two interferograms [10]. In 2016, Liu et al. proposed a PSA based on Lissajous figure and ellipse fitting technology, it can simultaneously extract the tested phase and phase shift from only two interferograms [11]. But these two algorithms both need pre-filtering. From 2011 to 2017, Vargas et al. proposed a series of PSAs based on principal component analysis (PCA) [12–16]. PCA is an efficient technique for phase extraction by converting a set of possibly correlated variables into a set of values of uncorrelated variables. But it needs more than three interferograms with the phase shift well distributed between 0 and 2π to subtract relatively accurate mean-background intensity. Hence, the more the interferograms, the higher the accuracy is. However, more interferograms will cost more acquisition time and computational time. So it is difficult to obtain the high accuracy and high speed simultaneously. In 2012, Vargas et al. presented a two-step demodulation based on the Gram-Schmidt orthonormalization method (GS), it requires subtracting the DC term by filtering before performing GS [17]. In the same year, Deng presented a two-step demodulation algorithm based on extreme value of the interference (EVI), the DC component also needs to be filtered out by a high-pass filter before performing EVI [18]. In 2015, Luo et al. proposed an advanced two-step phase demodulation algorithm based on the orthogonality of diamond diagonal vectors (DDV) [19]. And in the same year, Niu et al. proposed a two-step PSA based on the quotient of inner products of phase shifted interferograms (QIP), only the cosine of the phase shift can be obtained [20]. If the phase shift is more than π, the accurate phase distribution can't be obtained. The above two PSAs also need pre-filtering. In 2018,

* Corresponding author.
E-mail address: 521zhangyu2008@163.com (Y. Zhang).

https://doi.org/10.1016/j.optlaseng.2020.106134
Received 10 February 2020; Received in revised form 8 April 2020; Accepted 13 April 2020
Available online 12 May 2020
0143-8166/

Cheng et al. introduced a fast and accurate wavefront reconstruction method for two-frame PSI [21]. It also uses the high-pass Gaussian filter firstly before perform the phase retrieval. The cosine value of the unknown phase shift is estimated directly by solving a quartic polynomial equation, and then the phase map is readily reconstructed.

From the above literatures, we found some phenomenons. Firstly, some PSAs can only obtain the cosine value of phase shift, the range of phase shift is limited between 0 and π, hence these PSAs are not real random PSAs. Then, many PSAs need pre-filtering before the phase extraction, the pre-filtering process will cost more time and affect the accuracy. Lastly, some PSAs which don't need pre-filtering may need more than three interferograms, they will also spend more time. Generally, the PSAs with more than three interferograms have high accuracy and low speed, and the PSAs with two interferograms have high speed and low accuracy. It is difficult to obtain the high accuracy and speed simultaneously. To balance the computational time and accuracy, the research of non-iterative random PSA with two interferograms and no pre-filtering is essential.

In this paper, we will discuss a two-step random and non-iterative PSA . Section 2 presents the principle and process of the proposed PSA based on advanced principal component analysis and Lissajous ellipse fitting (APCA-LEF). In Section 3 the simulation of APCA-LEF is discussed, and the comparison of APCA-LEF with GS and EVI is performed. Section 4 evaluates the novel APCA-LEF with the experimental data. The conclusion is finally drawn in Section 5.

2. Principles

The intensity expression of the n^{th} phase shifted interferogram is

$$I_n(x,y) = a_n(x,y) + b_n(x,y)\cos\left(\varphi(x,y) + \delta_n\right) + \xi_n(x,y). \tag{1}$$

where $I_n(x, y)$ is the n^{th} phase shifted interferogram with the size of $N_x \times N_y$, n=1,2,...,N represents the image index with N the total number of phase shifted interferograms, N is set to 2 in this paper. $a_n(x, y)$ and $b_n(x, y)$ respectively represent the background intensity and modulation amplitude of the phase shifted interferograms. $\varphi(x, y)$ is the tested phase, δ_n is the phase shift, and$\xi_n(x, y)$ is the noise. For convenience, the spatial coordinate has been omitted in the following.

Eq. (1) can be rewritten as

$$I_n = \alpha_n I_c + \beta_n I_s + \kappa_n. \tag{2}$$

where $\alpha_n = \cos(\delta_n), \beta_n = -\sin(\delta_n), I_c = b_n\cos(\varphi)$, $I_s = b_n\sin(\varphi)$ and $\kappa_n = a_n + \xi_n$.

General PCA needs to filter the background intensity$a_n$and noise$\xi_n$by subtracting the average of all the phase shifted interferograms. However, the background intensity and noise can be well eliminated only when the phase shift is well distributed between 0 and 2π and the number of the phase shifted interferograms is large enough. More interferograms cost more acquisition time and computational time, and the well distributed phase shift is difficult to set because of the phase shift error. When the phase shift is "randomly" distributed and the number of phase shifted interferograms is small, the phase extracted by PCA will be not accurate. Especially when there are only two phase shifted interferograms, the real phase can't be extracted by PCA since the background intensity can't be eliminated in this situation. Hence, to ensure the accuracy and high speed simultaneously, we design a new method based on advanced principal component analysis and Lissajous ellipse fitting (APCA-LEF). It only needs two randomly phase shifted interferograms. APCA uses the adjacent pixels to suppress the effect of noise, and LEF can extract the accurate phase without the background intensity filtering.

The intensity of adjacent pixel can be showed as:

$$I_n(x+1,y) = I_n(x,y) + \left(I_n(x+1,y) - I_n(x,y)\right) \approx I_n(x,y) + I_n'(x,y). \tag{3}$$

where $I_n'(x, y)$ denotes the spatial derivative of $I_n(x, y)$.

A data matrix$\tilde{I}$constructed from extended data vectors is considered, $\tilde{I}$ is defined by

$$\tilde{I} = \begin{bmatrix} I_1 & I_2 & I_1 + I_1' & I_2 + I_2' \end{bmatrix} = Q\Gamma + \Re. \tag{4}$$

where $\tilde{I}$ is a matrix with the size of $N_xN_y \times 2N$, the n^{th} column is taken columnwise from I_n, and the $2n^{\text{th}}$ is taken columnwise from $I_n + I_n'$. $\Re$is the background intensity and noise matrix with the size of $N_xN_y \times 2N$, the n^{th} column is taken columnwise from κ_n.

$$Q = \begin{bmatrix} p & q & p & q \end{bmatrix}. \tag{5}$$

where the size of Q is$N_xN_y \times 2N$, p and q are the column vectors with the size of $N_xN_y \times 1$whose elements are taken columnwise from$I_c$andI_s.

$$\Gamma = \begin{pmatrix} \cos(\delta_1) & \cos(\delta_2) & \cos(\delta_1) & \cos(\delta_2) \\ -\sin(\delta_1) & -\sin(\delta_2) & -\sin(\delta_1) & -\sin(\delta_2) \\ 0 & 0 & -\sin(\delta_1) & -\sin(\delta_2) \\ 0 & 0 & -\cos(\delta_1) & -\cos(\delta_2) \end{pmatrix}. \tag{6}$$

The covariance matrix C can be expressed as

$$C = \tilde{I}^T\tilde{I} = (Q\Gamma + \Re)^T(Q\Gamma + \Re) = \Gamma^TQ^TQ\Gamma + \Gamma^TQ^T\Re + \Re^TQ\Gamma + \Re^T\Re \approx \Gamma^TQ^TQ\Gamma + \Re^T\Re. \tag{7}$$

The product of two uncorrelated matrixes-$\Gamma^TQ^T\Re$ and $\Re^TQ\Gamma$can be ignored because they are significantly smaller than $\Gamma^TQ^TQ\Gamma$ and $\Re^T\Re$.

$$\Gamma\Gamma^T = \begin{pmatrix} 2\sum_{n=1}^{N}\cos^2(\delta_n) & -2\sum_{n=1}^{N}\cos(\delta_n)\sin(\delta_n) & -\sum_{n=1}^{N}\cos(\delta_n)\sin(\delta_n) & -\sum_{n=1}^{N}\cos^2(\delta_n) \\ -2\sum_{n=1}^{N}\cos(\delta_n)\sin(\delta_n) & 2\sum_{n=1}^{N}\sin^2(\delta_n) & \sum_{n=1}^{N}\sin^2(\delta_n) & \sum_{n=1}^{N}\cos(\delta_n)\sin(\delta_n) \\ -\sum_{n=1}^{N}\cos(\delta_n)\sin(\delta_n) & \sum_{n=1}^{N}\sin^2(\delta_n) & \sum_{n=1}^{N}\sin^2(\delta_n) & \sum_{n=1}^{N}\cos(\delta_n)\sin(\delta_n) \\ -\sum_{n=1}^{N}\cos^2(\delta_n) & \sum_{n=1}^{N}\cos(\delta_n)\sin(\delta_n) & \sum_{n=1}^{N}\cos(\delta_n)\sin(\delta_n) & \sum_{n=1}^{N}\cos^2(\delta_n) \end{pmatrix}. \tag{8}$$

Note that, $\Gamma\Gamma^T$ is real and symmetric matrix, it can be diagonalized as$\Gamma\Gamma^T = P_\Gamma^T D_\Gamma P_\Gamma$, where $D_\Gamma$and $P_\Gamma$are diagonal and orthogonal matrices.

$$\Gamma\Gamma^T = P_\Gamma^T D_\Gamma P_\Gamma = \left(P_\Gamma^T {D_\Gamma}^{1/2}\hat{\Gamma}\right)\left(\hat{\Gamma}^T\left({D_\Gamma}^{1/2}\right)^T P_\Gamma\right)^T. \tag{9}$$

$\hat{\Gamma}$is a new matrix that $\hat{\Gamma}\hat{\Gamma}^T = E$, where$E$is unit matrix. Hence, according to Eq. (9), we can get the expression of Γas

$$\Gamma = P_\Gamma^T {D_\Gamma}^{1/2}\hat{\Gamma}. \tag{10}$$

The new matrix$\hat{\Gamma}$ can be expressed as

$$\hat{\Gamma} = {D_\Gamma}^{-1/2} P_\Gamma \Gamma. \tag{11}$$

The$D_\Gamma$is given by

$$D_\Gamma = \begin{pmatrix} \lambda_1 & 0 & 0 & 0 \\ 0 & \lambda_2 & 0 & 0 \\ 0 & 0 & \lambda_3 & 0 \\ 0 & 0 & 0 & \lambda_4 \end{pmatrix}. \tag{12}$$

where$\lambda_i (i = 1, 2, 3, 4)$ is the eigenvalue of $\Gamma\Gamma^T$.

We know thatP_Γ^T is a 4×4 orthogonal matrix, so it can be expressed as

$$P_\Gamma^T = \begin{pmatrix} \cos(\theta) & \sin(\theta) & 0 & 0 \\ -\sin(\theta) & \cos(\theta) & 0 & 0 \\ 0 & 0 & \cos(\theta) & \sin(\theta) \\ 0 & 0 & -\sin(\theta) & \cos(\theta) \end{pmatrix}. \tag{13}$$

Additionally, $Q^T Q$ can be expressed as

$$\begin{aligned} Q^T Q &= \begin{pmatrix} p \\ q \\ p \\ q \end{pmatrix}\begin{pmatrix} p & q & p & q \end{pmatrix} = \begin{pmatrix} \|p\|^2 & \langle p\cdot q\rangle & \|p\|^2 & \langle p\cdot q\rangle \\ \langle p\cdot q\rangle & \|q\|^2 & \langle p\cdot q\rangle & \|q\|^2 \\ \|p\|^2 & \langle p\cdot q\rangle & \|p\|^2 & \langle p\cdot q\rangle \\ \langle p\cdot q\rangle & \|q\|^2 & \langle p\cdot q\rangle & \|q\|^2 \end{pmatrix} \\ &= \sum_{N_x\times N_y}\begin{pmatrix} b^2\cos^2(\varphi) & b^2\cos(\varphi)\sin(\varphi) & b^2\cos^2(\varphi) & b\cos(\varphi)\sin(\varphi) \\ b^2\cos(\varphi)\sin(\varphi) & b^2\sin^2(\varphi) & b^2\cos(\varphi)\sin(\varphi) & b^2\sin^2(\varphi) \\ b^2\cos^2(\varphi) & b^2\cos(\varphi)\sin(\varphi) & b^2\cos^2(\varphi) & b^2\cos(\varphi)\sin(\varphi) \\ b^2\cos(\varphi)\sin(\varphi) & b^2\sin^2(\varphi) & b^2\cos(\varphi)\sin(\varphi) & b^2\sin^2(\varphi) \end{pmatrix}. \end{aligned} \tag{14}$$

where b and φrespectively represent $b(x, y)$ and $\varphi(x, y)$.

If we have more than one fringe in the interferograms, we can use the approximation

$$\sum_{N_x\times N_y} b^2\cos(\varphi)\sin(\varphi) \approx 0. \tag{15}$$

and

$$\sum_{N_x\times N_y} b^2\cos^2(\varphi) \approx \sum_{N_x\times N_y} b^2\sin^2(\varphi) \approx \sigma. \tag{16}$$

Hence, Eq. (14) can be rewritten as

$$Q^T Q = S_Q \approx \sigma\begin{pmatrix} 1 & 0 & 1 & 0 \\ 0 & 1 & 0 & 1 \\ 1 & 0 & 1 & 0 \\ 0 & 1 & 0 & 1 \end{pmatrix}. \tag{17}$$

According to Eqs. (7), (10) and (17), we have

$$C \approx \hat{\Gamma}^T {D_\Gamma}^{1/2} P_\Gamma S_Q P_\Gamma^T {D_\Gamma}^{1/2}\hat{\Gamma} + \Re^T\Re = \hat{\Gamma}^T\left({D_\Gamma}^{1/2} P_\Gamma S_Q P_\Gamma^T {D_\Gamma}^{1/2}\right)\hat{\Gamma} + \Re^T\Re = \hat{\Gamma}^T B\hat{\Gamma} + \Re^T\Re. \tag{18}$$

where $B = {D_\Gamma}^{1/2} P_\Gamma S_Q P_\Gamma^T {D_\Gamma}^{1/2} = \sigma\begin{pmatrix} \lambda_1 & 0 & {\lambda_1}^{1/2}{\lambda_3}^{1/2} & 0 \\ 0 & \lambda_2 & 0 & {\lambda_2}^{1/2}{\lambda_4}^{1/2} \\ {\lambda_1}^{1/2}{\lambda_3}^{1/2} & 0 & \lambda_3 & 0 \\ 0 & {\lambda_2}^{1/2}{\lambda_4}^{1/2} & 0 & \lambda_4 \end{pmatrix}$.

We can see that B is a real and symmetric matrix, so it can be diagonalized as $P^T D_Q P$, where $D_Q$and P are diagonal and orthogonal matrices, they can be expressed as

$$D_Q = \sigma\begin{pmatrix} \lambda_1+\lambda_3 & 0 & 0 & 0 \\ 0 & \lambda_2+\lambda_4 & 0 & 0 \\ 0 & 0 & 0 & 0 \\ 0 & 0 & 0 & 0 \end{pmatrix}. \tag{19}$$

$$P = \begin{pmatrix} 1 & 0 & 1 & 0 \\ 0 & 1 & 0 & 1 \\ {\lambda_1}^{-1/2}{\lambda_3}^{1/2} & 0 & -{\lambda_1}^{1/2}{\lambda_3}^{-1/2} & 0 \\ 0 & {\lambda_2}^{-1/2}{\lambda_4}^{1/2} & 0 & -{\lambda_2}^{1/2}{\lambda_4}^{-1/2} \end{pmatrix}. \tag{20}$$

Eq. (18) can be rewritten as

$$C \approx \hat{\Gamma}^T\left(P^T D_Q P + P^T D_{\Re} P\right)\hat{\Gamma}=\left(P\hat{\Gamma}\right)^T\left(D_Q + D_{\Re}\right)\left(P\hat{\Gamma}\right). \tag{21}$$

where

$$\Re^T\Re = \left(P\hat{\Gamma}\right)^T\left(\Re\hat{\Gamma}^T P^T\right)^T\left(\Re\hat{\Gamma}^T P^T\right)\left(P\hat{\Gamma}\right) = \left(P\hat{\Gamma}\right)^T D_{\Re}\left(P\hat{\Gamma}\right). \tag{22}$$

According to Eq. (10), Eq. (4) can be rewritten as

$$\tilde{I}=Q\left(P_\Gamma^T {D_\Gamma}^{1/2}\hat{\Gamma}\right) + \Re = \left(QP_\Gamma^T\right){D_\Gamma}^{1/2}\hat{\Gamma} + \Re. \tag{23}$$

PCA is a technique from statistics for reducing an image or dataset that transforms a number of uncorrelated images into the smallest number uncorrelated images called the principle components. Since the covariance matrix C is a real and symmetric matrix, it can be diagonalized as

$$C = U^T DU. \tag{24}$$

where U and D are orthogonal and diagonal matrices.

The principle components of the interferograms are given by

$$Z = \tilde{I}U^T. \tag{25}$$

where Z is matrix with the size of $N_xN_y \times 2N$, and its column vectors z_n are the principle components.

According to Eqs. (21) and (23), we can state that U and D correspond to $P\hat{\Gamma}$ and $D_Q + D_{\Re}$ respectively. Then, we can rewrite Eq. (25) as

$$Z = \tilde{I}\left(P\hat{\Gamma}\right)^T = \left(QP_\Gamma^T\right){D_\Gamma}^{1/2}P^T + \Re\hat{\Gamma}^T P^T = \hat{Q}{D_\Gamma}^{1/2}P^T + \Re\hat{\Gamma}^T P^T. \tag{26}$$

where $\hat{Q} = QP_\Gamma^T$.

$\hat{Q}$ can be further calculated by

$$\hat{Q} = QP_\Gamma^T = \begin{pmatrix} p & q & p & q \end{pmatrix}\begin{pmatrix} \cos(\theta) & \sin(\theta) & 0 & 0 \\ -\sin(\theta) & \cos(\theta) & 0 & 0 \\ 0 & 0 & \cos(\theta) & \sin(\theta) \\ 0 & 0 & -\sin(\theta) & \cos(\theta) \end{pmatrix} = \begin{pmatrix} \hat{p} & \hat{q} & \hat{p} & \hat{q} \end{pmatrix}. \tag{27}$$

where $\hat{p}$ and $\hat{q}$ are column vectors with the size of $N_xN_y \times 1$ whose elements are taken columnwise from $b\cos(\varphi+\theta)$ and $b\sin(\varphi+\theta)$.

According Eqs. (12), (20) and (27), we can rewrite Eq. (26) as

$$\begin{aligned} Z &= \begin{pmatrix} \hat{p} & \hat{q} & \hat{p} & \hat{q} \end{pmatrix}\begin{pmatrix} {\lambda_1}^{1/2} & 0 & 0 & 0 \\ 0 & {\lambda_2}^{1/2} & 0 & 0 \\ 0 & 0 & {\lambda_3}^{1/2} & 0 \\ 0 & 0 & 0 & {\lambda_4}^{1/2} \end{pmatrix}\begin{pmatrix} 1 & 0 & {\lambda_1}^{-1/2}{\lambda_3}^{1/2} & 0 \\ 0 & 1 & 0 & {\lambda_2}^{-1/2}{\lambda_4}^{1/2} \\ 1 & 0 & -{\lambda_1}^{1/2}{\lambda_3}^{-1/2} & 0 \\ 0 & 1 & 0 & -{\lambda_2}^{1/2}{\lambda_4}^{-1/2} \end{pmatrix} + \begin{pmatrix} \left(\Re\hat{\Gamma}^T P^T\right)_1 \\ \left(\Re\hat{\Gamma}^T P^T\right)_2 \\ \left(\Re\hat{\Gamma}^T P^T\right)_3 \\ \left(\Re\hat{\Gamma}^T P^T\right)_4 \end{pmatrix}^T \\ &= \begin{pmatrix} \hat{p}\left({\lambda_1}^{1/2} + {\lambda_3}^{1/2}\right) \\ \hat{q}\left({\lambda_2}^{1/2} + {\lambda_4}^{1/2}\right) \\ \hat{p}\left({\lambda_3}^{1/2} - {\lambda_1}^{1/2}\right) \\ \hat{q}\left({\lambda_4}^{1/2} - {\lambda_2}^{1/2}\right) \end{pmatrix}^T + \begin{pmatrix} \left(\Re\hat{\Gamma}^T P^T\right)_1 \\ \left(\Re\hat{\Gamma}^T P^T\right)_2 \\ \left(\Re\hat{\Gamma}^T P^T\right)_3 \\ \left(\Re\hat{\Gamma}^T P^T\right)_4 \end{pmatrix}^T \end{aligned}. \tag{28}$$

Then,

$$\begin{aligned} z_1 &= \hat{p}\left({\lambda_1}^{1/2} + {\lambda_3}^{1/2}\right) + \left(\Re\hat{\Gamma}^T P^T\right)_1 = b\cos(\varphi+\theta)\left({\lambda_1}^{1/2} + {\lambda_3}^{1/2}\right) + \left(\Re\hat{\Gamma}^T P^T\right)_1 \\ z_2 &= \hat{q}\left({\lambda_2}^{1/2} + {\lambda_4}^{1/2}\right) + \left(\Re\hat{\Gamma}^T P^T\right)_2 = b\sin(\varphi+\theta)\left({\lambda_2}^{1/2} + {\lambda_4}^{1/2}\right) + \left(\Re\hat{\Gamma}^T P^T\right)_2 \\ z_3 &= \hat{p}\left({\lambda_3}^{1/2} - {\lambda_1}^{1/2}\right) + \left(\Re\hat{\Gamma}^T P^T\right)_3 = b\cos(\varphi+\theta)\left({\lambda_3}^{1/2} - {\lambda_1}^{1/2}\right) + \left(\Re\hat{\Gamma}^T P^T\right)_3 \\ z_4 &= \hat{q}\left({\lambda_4}^{1/2} - {\lambda_2}^{1/2}\right) + \left(\Re\hat{\Gamma}^T P^T\right)_4 = b\sin(\varphi+\theta)\left({\lambda_4}^{1/2} - {\lambda_2}^{1/2}\right) + \left(\Re\hat{\Gamma}^T P^T\right)_4 \end{aligned}. \tag{29}$$

The first and second components (z_1 and z_2) that corresponds to the highest eigenvalues can be obtained by PCA.

Then we can obtain

$$\begin{aligned} \cos(\varphi+\theta) &= \frac{z_1 - \left(\Re\hat{\Gamma}^T P^T\right)_1}{b\left({\lambda_1}^{1/2} + {\lambda_3}^{1/2}\right)} \\ \sin(\varphi+\theta) &= \frac{z_2 - \left(\Re\hat{\Gamma}^T P^T\right)_2}{b\left({\lambda_2}^{1/2} + {\lambda_4}^{1/2}\right)} \end{aligned}. \tag{30}$$

Because $\sin^2(\varphi+\theta) + \cos^2(\varphi+\theta) = 1$, and we use X and Y instead of z_2 and z_1, then Eq. (30) can be rewritten as

$$\left(\frac{X - x_0}{a_x}\right)^2 + \left(\frac{Y - y_0}{a_y}\right)^2 = 1. \tag{31}$$

Note that Eq. (31) is just an ellipse equation,

$$a_x = b\left({\lambda_2}^{1/2} + {\lambda_4}^{1/2}\right), a_y = b\left({\lambda_1}^{1/2} + {\lambda_3}^{1/2}\right), x_0 = \left(\Re\hat{\Gamma}^T P^T\right)_2, y_0 = \left(\Re\hat{\Gamma}^T P^T\right)_1. \tag{32}$$

Eq. (31) can be expanded as a general conic function:

$$\frac{1}{{a_x}^2}X^2 + \frac{1}{{a_y}^2}Y^2 - 2\frac{x_0}{{a_x}^2}X - 2\frac{y_0}{{a_y}^2}Y + \frac{{x_0}^2}{{a_x}^2} + \frac{{y_0}^2}{{a_y}^2} - 1 = 0. \tag{33}$$

A general conic function can be also expressed by the following second order polynomial:

$$F = cx^2 + dxy + ey^2 + fx + gy + h. \tag{34}$$

For an ellipse, Eq. (34) needs to meet the conditions of $F = 0$ and $d^2 - 4ce < 0$. In the following, the real phase distribution will be obtained by the Lissajous ellipse fitting (LEF) method. It will be easy to calculate the conic coefficients of Eq. (34) by the least squares algorithm, the semi-major amplitudea_x, semi-minor amplitudea_y, the center offset $x_0$andy_0 can be calculated as

$$a_x = \sqrt{2\frac{cg^2 + ef^2 + hd^2 - dfg - 4ceh}{(d^2 - 4ce)\left(\sqrt{(c-e)^2 + d^2} - (c+e)\right)}}, a_y = \sqrt{2\frac{cg^2 + ef^2 + hd^2 - dfg - 4ceh}{(d^2 - 4ce)\left(-\sqrt{(c-e)^2 + d^2} - (c+e)\right)}}.$$
$$x_0 = \frac{2ef - dg}{d^2 - 4ce}, y_0 = \frac{2cg - df}{d^2 - 4ce} \tag{35}$$

Lastly, according to Eqs. (30) and (31), the phase Φ can be easily calculated as

$$\Phi = \varphi + \theta = \tan^{-1}\left(\frac{X - x_0}{Y - y_0} \cdot \frac{a_y}{a_x}\right). \tag{36}$$

We know that there is only a constant θ between betweenφandΦ, which doesn't affect the whole phase distribution, hence we can use Φ to express the tested phase distribution.

For the two step PSAs, the number of unknowns is more than that of equations, so the background intensity needs to be removed by some methods, otherwise the phase can't be obtained. Generally, many two-step PSAs utilize the filtering algorithm to remove the background intensity, but when the noise is large, the filtering algorithm can't distinguish the signal and noise, even though the noise is small, the filtering error is also unavoidable. The proposed method can extract the phase distribution from two randomly phase shifted interferograms without background intensity filtering. APCA can eliminate part of noise by the adjacent pixels. Although LEF can't eliminate noise, the relatively accurate semi-major amplitudea_x, semi-minor amplitudea_y, the center offset $x_0$andy_0 can be calculated by the LEF process, then the background intensity can be removed by transform the ellipse to the an approximate circle with $(X - x_0)/a_x$as the x coordinate and $(Y - y_0)/a_y$as the y coordinate centered at the origin. Finally the relatively accurate phase can be calculated.

In the following, we will introduce the process of the proposed method in detail:

1) Generate an extended matrix $\tilde{I}$ with the size of$N_xN_y \times 2N$, where the nth column is taken columnwise from the intensity of nth phase shifted interferogramsI_n, and 2nth column is taken columnwise from the adjacent pixels intensity of nth phase shifted interferogramsI_n+$I_n{}'$;
2) calculate the covariance matrix C by equation$C = \tilde{I}^T\tilde{I}$;
3) calculate the orthogonal matrix $P\hat{\Gamma}$ including the eigenvectors of the covariance matrix C;
4) obtain the first and second principle components (z_1 and z_2) which corresponds to the highest eigenvalues by $Z = \tilde{I}(P\hat{\Gamma})^T$;
5) plot an approximate ellipse with z_2 as the x coordinate and z_1 as the y coordinate;
6) calculate the semi-major amplitude a_x, semi-minor amplitude a_y, the center offset $x_0$andy_0 of the Lissajous ellipse by the LEF process;
7) calculate the phase distribution.

Theoretically, the proposed method could eliminate more noise when more adjacent pixels are integrated in the extended data matrix. In addition, geometry of the adjacent pixels also has impact on the accuracy of result. In the following, M is the number of adjacent pixels.

For example, for M = 2, let I^* be a 2N dimensional row vector defined by

$$I^*{}_{x,y} = \left(I_1(x,y), I_2(x,y)\right). \tag{37}$$

and let $\hat{I}$ be a 4N dimensional row vector defined by

$$\hat{I}_{x,y} = \left(I^*{}_{x,y}, I^*{}_{x+1,y}\right) = \left(I_1(x,y), I_2(x,y), I_1(x+1,y), I_2(x+1,y)\right). \tag{38}$$

A data matrix $\tilde{I}$is constructed by concatenating $\hat{I}_{x,y}$ for every pixels vertically,

$$\tilde{I} = \left(\hat{I}_{1,1}, \hat{I}_{2,1}, \cdots, \hat{I}_{N_x,1}, \hat{I}_{1,2}, \hat{I}_{2,2}, \cdots, \hat{I}_{N_x,N_y}\right)^T. \tag{39}$$

Eight $\hat{I}_{x,y}$with different M used in the simulations and experiments are expressed in the following and shown in Fig. 1.

Situation 1:M = 1

$$\hat{I}_{x,y} = I^*{}_{x,y} \tag{40}$$

Situation 2:M = 2

$$\hat{I}_{x,y} = \left(I^*{}_{x,y}, I^*{}_{x+1,y}\right). \tag{41}$$

Situation 3:M = 3,

$$\hat{I}_{x,y} = \left(I^*{}_{x,y}, I^*{}_{x+1,y}, I^*{}_{x-1,y}\right). \tag{42}$$

Situation 4:M = 5,

$$\hat{I}_{x,y} = \left(I^*{}_{x,y}, I^*{}_{x+1,y}, I^*{}_{x-1,y}, I^*{}_{x,y+1}, I^*{}_{x,y-1}\right). \tag{43}$$

Situation 5:M = 9,

$$\hat{I}_{x,y} = \left(I^*{}_{x,y}, I^*{}_{x+1,y}, I^*{}_{x-1,y}, I^*{}_{x,y+1}, I^*{}_{x,y-1}, I^*{}_{x+1,y+1}, I^*{}_{x+1,y-1}, I^*{}_{x-1,y+1}, I^*{}_{x-1,y-1}\right). \tag{44}$$

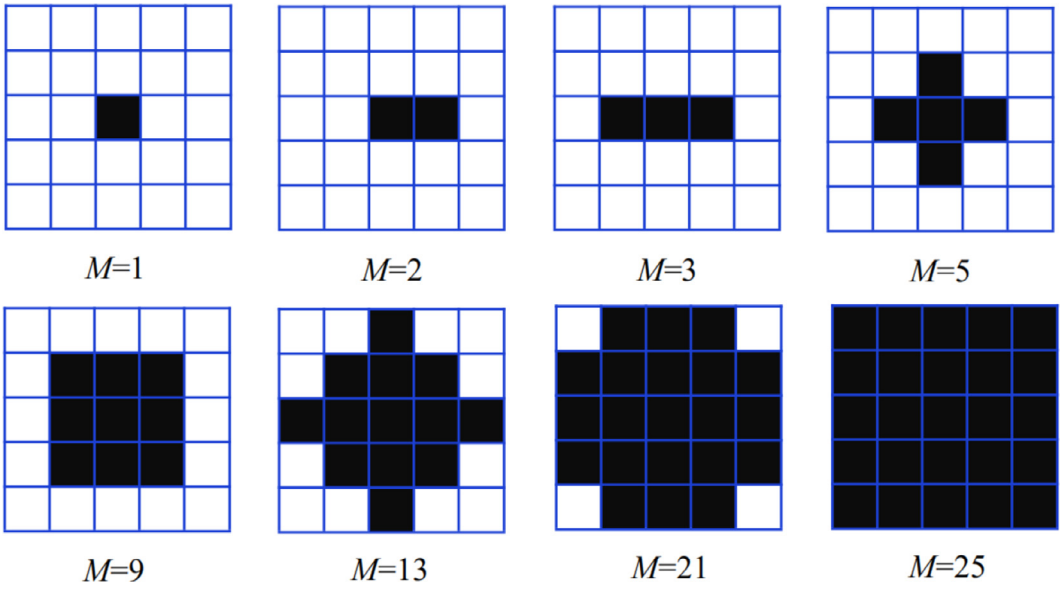

Fig. 1. A schematic diagram of different adjacent pixels, where pixels are colored by black.

Situation 6:M = 13,

$$\hat{I}_{x,y} = \left(I^*_{x,y}, I^*_{x+1,y}, I^*_{x-1,y}, I^*_{x,y+1}, I^*_{x,y-1}, I^*_{x+1,y+1}, I^*_{x+1,y-1}, I^*_{x-1,y+1}, I^*_{x-1,y-1}, I^*_{x+2,y}, I^*_{x-2,y}, I^*_{x,y+2}, I^*_{x,y-2}\right). \quad (45)$$

Situation 7:M = 21,

$$\hat{I}_{x,y} = \left(I^*_{x,y}, I^*_{x+1,y}, I^*_{x-1,y}, I^*_{x,y+1}, I^*_{x,y-1}, I^*_{x+1,y+1}, I^*_{x+1,y-1}, I^*_{x-1,y+1}, I^*_{x-1,y-1}, I^*_{x+2,y}, I^*_{x-2,y}, I^*_{x,y+2}, I^*_{x,y-2}, I^*_{x+2,y+1}, I^*_{x+2,y-1}, I^*_{x-2,y+1}, I^*_{x-2,y-1}, I^*_{x+1,y+2}, I^*_{x-1,y+2} I^*_{x+1,y-2}, I^*_{x-1,y-2}\right). \quad (46)$$

Situation 8:M = 25,

$$\hat{I}_{x,y} = \left(I^*_{x,y}, I^*_{x+1,y}, I^*_{x-1,y}, I^*_{x,y+1}, I^*_{x,y-1}, I^*_{x+1,y+1}, I^*_{x+1,y-1}, I^*_{x-1,y+1}, I^*_{x-1,y-1}, I^*_{x+2,y}, I^*_{x-2,y}, I^*_{x,y+2}, I^*_{x,y-2}, I^*_{x+2,y+1}, I^*_{x+2,y-1}, I^*_{x-2,y+1}, I^*_{x-2,y-1}, I^*_{x+1,y+2}, I^*_{x-1,y+2}, I^*_{x+1,y-2}, I^*_{x-1,y-2}, I^*_{x+2,y+2}, I^*_{x+2,y-2}, I^*_{x-2,y+2}, I^*_{x-2,y-2}\right). \quad (47)$$

Note that the boundary of phase shifted interferograms must be extended properly so that M adjacent pixels are valid, such as $I^*_{N_x+1,N_y}$ is out of the range of phase shifted interferograms. According to the above eight situations, we extended the size of the phase shifted interferograms from $N_x \times N_y$ to $(N_x+4)\times(N_y+4)$. The values of 1st and 2nd rows for the extended interferograms with the size of $(N_x+4)\times(N_y+4)$ are same as that of the 1st row for the original interferogram with the size of $N_x \times N_y$. The values of $(N_x+3)^{\text{th}}$ and $(N_x+4)^{\text{th}}$ rows for the extended interferograms are same as that of the $N_x{}^{\text{th}}$ row for the original interferogram. Moreover, the values of 3rd to $(N_x+2)^{\text{th}}$ rows for the extended interferograms are same as that of 1st to $N_x$rows for the original interferogram. Finally, the extension of the column is same as the row.

3. Simulation

To verify the effectiveness of the method proposed above, we perform a series of numerical simulations, and compare it with two well-evaluated two-step random PSAs-GS and EVI. Note that, the Hilbert-Huang pre-filtering will be performed before using GS and EVI. In the following, all computations are performed with the CPU of Intel(R) Core(TM) i5-8265U and the 8 GB memory, and we use the Matlab software for coding.

Firstly, we perform APCA-LEF, GS and EVI to process two phase shifted interferograms with the circular fringes. In the following, the tested phase is set as$\varphi = N_f \pi(x^2+y^2)$, in which $N_f = 5$ is the fringe number in the interferogram. Fig. 2(a) shows the theoretical phase distribution. The background intensity and modulation amplitude are set as $a_i(x,y) = N_a \exp[-0.02(x^2+y^2)]$and $b_i(x,y) = N_b \exp[-0.02(x^2+y^2)]$ respectively. Both the fluctuation and non-uniformity of the background intensity and modulation amplitude exist, hence, N_a of the 1st and 2nd interferograms are set as 1 and 0.95, N_b of the 1st and 2nd interferograms are set as 0.9 and 0.85. Moreover, we add noise generated by the function *awgn* in Matlab to the phase shifted interferograms. With the above parameters setting, two simulated phase shifted interferograms with the size of 401 × 401, SNR of 20 dB and the phase shift of 1 rad are generated, as shown in Fig. 2(c) and 2(d).

Fig. 3 show the phase error distributions calculated by APCA-LEF with different M. When M = 1, APCA-LEF method returned back to the original PCA-LEF method with no adjacent pixels involved, the extracted phase distribution is shown in Fig. 2(b), in this situation, the RMS phase error is largest. We can see that, for 20 dB of noise, the larger the M, the smaller the RMS phase error is, and the RMS phase error in the situation of M = 1 is more than 10 times of that in the situation of M = 25, that is to say, the proposed method can suppress the effect of noise with the adjacent pixels, and the result is remarkable. Moreover, when M is less than 5, the RMS phase error decreases largely with the increase of M, but when M is larger than 5, the RMS phase error decreases in a small degree with the increase of M. Fig. 4 show the ellipses before and after using LEF for APCA-LEF in the situation of M = 1. We can see that, before using LEF, the approximate ellipse with X as the x coordinate and Y as the y coordinate is not centered at the origin, after using LEF, the ellipse was transformed an approximate circle with $(X-x_0)/a_x$as the x coordinate and $(Y-y_0)/a_y$as the y coordinate centered at the origin, the curve is not smooth since the noise exists, and LEF cannot remove this effect.

In order to verify the outstanding performance of the proposed method, we compare it with the well-evaluated two-step PSAs-GS and EVI in the following. Fig. 5 shows the simulated results of the circular fringes using GS and EVI. We can see that the phase error distributions of them are similar because they both use the pre-filtering, and the filtering errors are similar. Moreover, the RMS phase errors of GS and EVI are respectively 0.1735 rad and 0.1787 rad which are larger than that of APCA-LEF with any M except M = 1. We can get the conclusion that APCA-LEF can obtain the higher accuracy with only two no pre-filtering phase shifted interferograms.

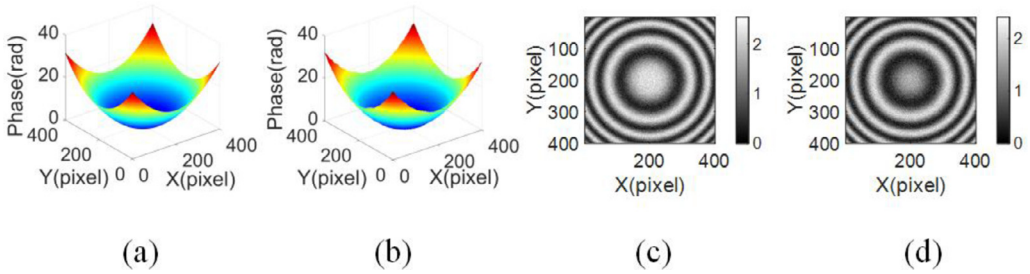

Fig. 2. Simulated phase distributions and two phase shifted interferograms with the circular fringes. (a) The theoretical phase distribution, (b) the phase distribution extracted by APCA-LEF in the situation of M = 1, (c) and (d) the first interferogram and the second interferogram.

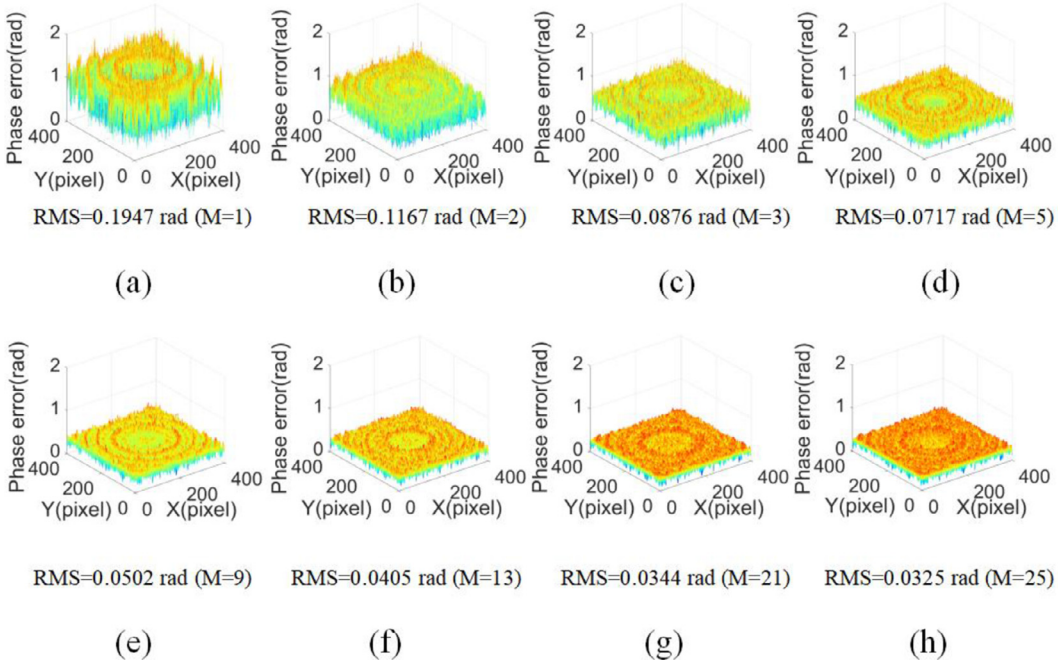

Fig. 3. The phase error distributions of the circular fringes using APCA-LEF with different M.

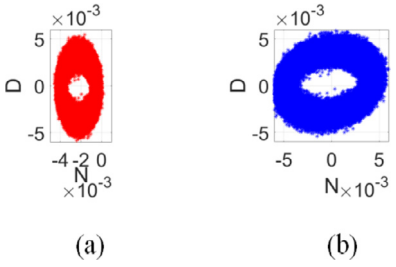

Fig. 4. The ellipses before and after using LEF for APCA-LEF in the situation of M = 1.

We know that two-step PSA is easily influenced by the noise, hence we estimate the noise effect to three different methods in the following, and different M for APCA-LEF are also studied. The SNR of noise is set from 20 dB to 70 dB, other parameters are same as the above simulation. We plot the RMS phase errors of the different levels of noises for APCA-LEF with different M, GS and EVI, as shown in Fig. 6. Since the large filtering error of GS and EVI, the RMS phase errors of GS and EVI are larger than that of APCA-LEF for any level of noise except APCA-LEF with 20dB of noise in the situation of M = 1. The RMS phase errors of GS and EVI are similar for the same level of noise. When the SNR of noise is less than 50 dB, the larger the noise, the larger the RMS phase

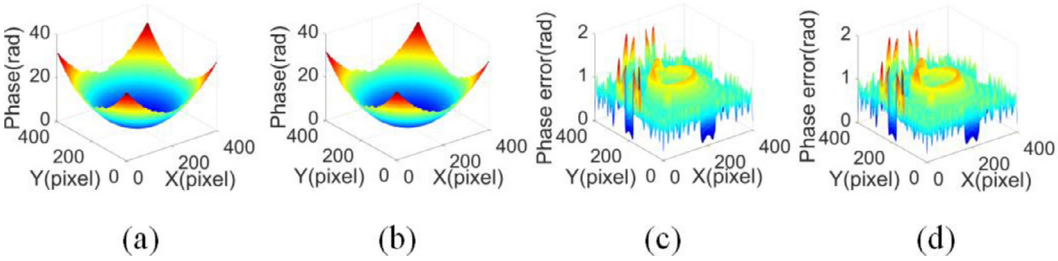

Fig. 5. Simulated results of the circular fringes using GS and EVI. (a) and (b) The phase distributions extracted by GS and EVI, (c) and (d) the phase error distributions of GS and EVI.

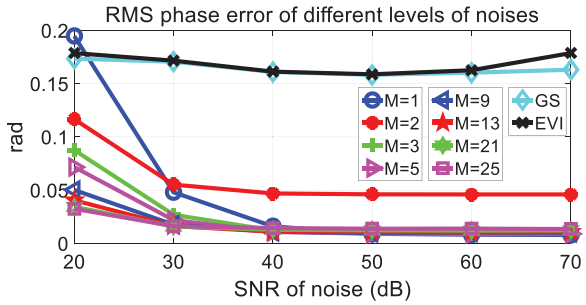

Fig. 6. RMS phase errors of different levels of noises for APCA-LEF with different M, GS and EVI.

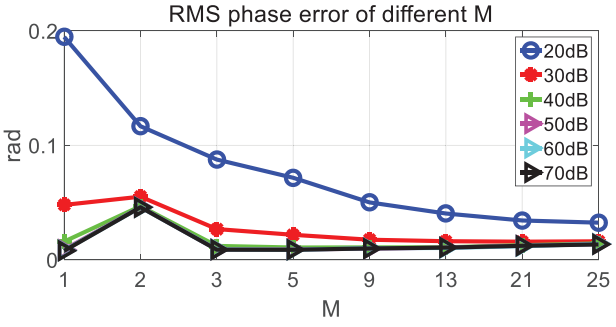

Fig. 7. RMS phase errors of different M for APCA-LEF.

error of GS and EVI is, and when the SNR of noise is more than 50 dB, the RMS phase error is ruleless because the effect of filtering error is larger than that of noise. For APCA-LEF, the larger the noise, the larger the RMS phase error is for any M. Moreover, the RMS phase errors of APCA-LEF are relatively small and stable when the SNR of noise is more than 50 dB, in this situation, the main phase error is caused by the non-uniform and variable background intensity, modulation amplitude and the intrinsic error of the algorithm.

In order to study the effect of different M to APCA-LEF, we plot the RMS phase errors of different M, as shown in Fig. 7. We find a strange phenomenon that, only when the SNR of noise is 20dB, the larger the M, the smaller the RMS phase error is, for other levels of noises, when M = 2, the RMS phase error is largest. When M = 2, there is a tilt error caused by the asymmetric geometry of the adjacent pixels, for other values of M, the adjacent pixels taken part in the APCA process are all symmetric, as shown in Fig. 1. When the SNR of noise is 20dB, the effect of noise and background intensity and modulation amplitude error called systematic error is larger than that of the tilt error, but when the SNR of noise is larger than 30 dB, the effect of the systematic error is less than that of the tilt error. We need to avoid the situation of M=2 because we don't know the SNR of noise in the practical situation. In addition, when the SNR of noise is 30 dB, the RMS phase error is decreasing with the increase of M except M = 2 and M = 25, the RMS phase error of M = 25 is only a little larger than that of M = 21 since the

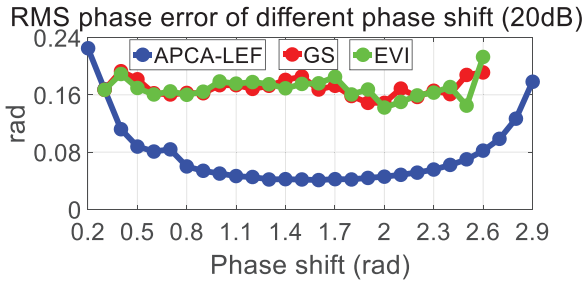

Fig. 8. The RMS phase errors of APCA-LEF, GS and EVI with different phase shifts.

effect of the adjacent pixels error is a little bigger than that of systematic error. Moreover, when the SNR of noise is more than 40 dB, the RMS phase error is decreasing with the increase of M when M is less than 5 except M = 2, and when M is more than 5, the RMS phase error is increasing with the increase of M since the effect of the adjacent pixels error is larger than that of the systematic error. From the above analysis, we can conclude that, when the SNR of noise is less than 30 dB, the best value of M is 21 or 25, when the SNR of noise is more than 40 dB, the best value of M is 5. Although the best M is different for the different levels of noises, we need to choose a relatively appropriate M to fit all of the situations since we don't know the SNR of noise in the practical situation. When the SNR of noise is less than 30 dB, the RMS phase errors in the situation of M = 5 are relatively smaller, hence we choose 5 as the most appropriate value of M for all the levels of noises.

To analyze the effects of different phase shifts to three different methods, we calculate the RMS phase errors of APCA-LEF, GS and EVI with different phase shifts and SNR of 20 dB, and we choose the situation of M = 5 for APCA-LEF in the following analysis, the results are shown in Fig. 8. For GS and EVI, the RMS phase errors are irrelevant to the different phase shifts since the effect of the filtering error is more larger than that of the different phase shifts. For APCA-LEF, the RMS phase errors are relevant to the different phase shifts, we found that the farther away the phase shift from 0 rad and π rad, the smaller the RMS phase error is, hence, if the high accuracy is required, the phase shift would be best to far away from 0 rad and π rad. Moreover, the range of phase shift for APCA-LEF which is between 0.2 rad and 2.9 rad is larger than that for GS and EVI which is between 0.3 rad and 2.6 rad. Last but not least, the accuracy of APCA-LEF is higher than that of GS and EVI for the whole range of phase shift since APCA-LEF uses the original phase shifted interferograms rather than phase shifted interferogram's after filtering, and the adjacent pixels taken part in APCA also improve the accuracy of APCA-LEF.

To verify the robustness of the proposed method, we also simulate the straight and complex fringes, the comparisons of APCA-LEF, GS and EVI are also performed in the following. For the straight fringes, the theoretical phase is set as$\varphi = 5\pi x$, and for the complex fringes, the phase is set as $\varphi = 5\pi x + 5peaks(401)$. The SNR of noise is 20 dB, and the phase shift is 1 rad, other parameters are same as the circular fringes. Fig. 9 shows the simulated phase distributions and two phase shifted

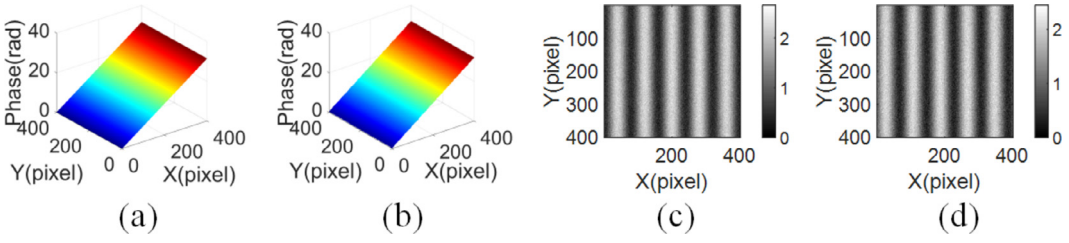

Fig. 9. Simulated phase distributions and two phase shifted interferograms with the straight fringes. (a) The theoretical phase distribution, (b) the phase distribution extracted by APCA-LEF in the situation of M = 1, (c) and (d) the first interferogram and the second interferogram.

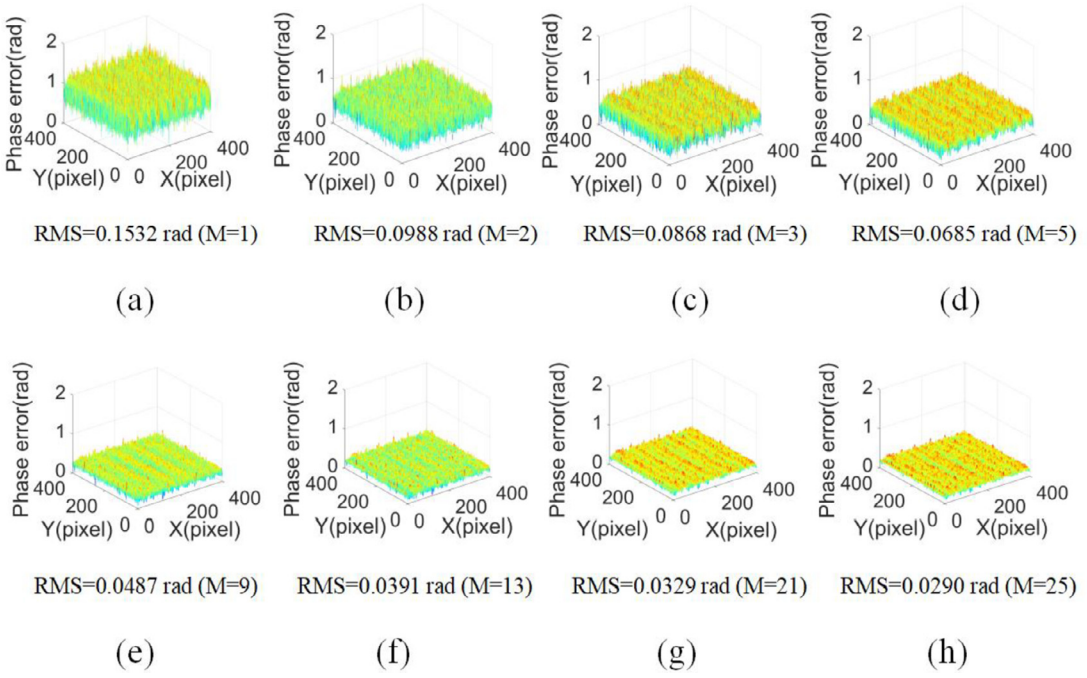

Fig. 10. The phase error distributions of the straight fringes using APCA-LEF with different M.

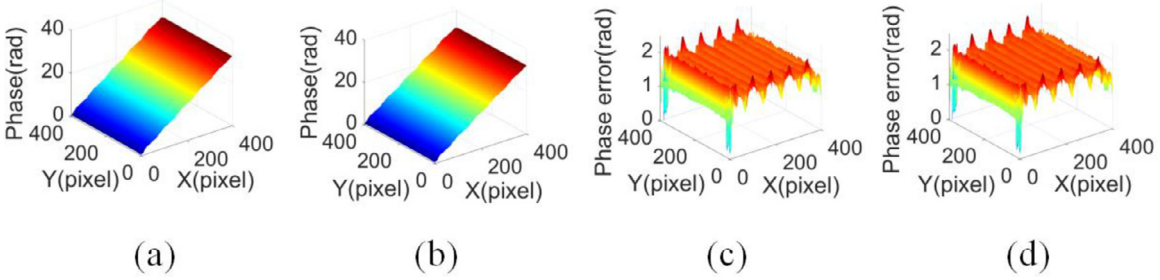

Fig. 11. Simulated results of the straight fringes using GS and EVI. (a) and (b) The phase distributions extracted by GS and EVI, (c) and (d) the phase error distributions of GS and EVI.

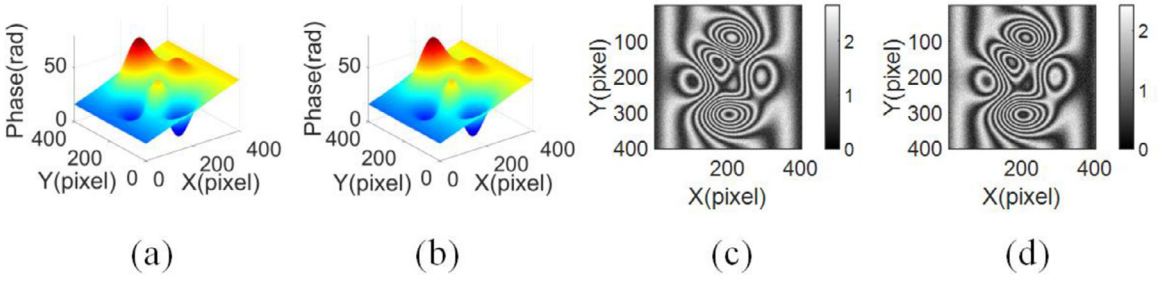

Fig. 12. Simulated phase distributions and two phase shifted interferograms with the complex fringes. (a) The theoretical phase distribution, (b) the phase distribution extracted by APCA-LEF in the situation of M = 1, (c) and (d) the first interferogram and the second interferogram.

interferograms with the straight fringes, and Figs. 10 and 11 present the simulated results of the straight fringes using APCA-LEF, GS and EVI. The simulated phase distributions and two phase shifted interferograms with the complex fringes are drawn in Fig. 12, we can see that the interferograms with the complex fringes are asymmetrical, and the simulated results of APCA-LEF, GS and EVI are shown in Figs. 13 and 14. Because the interferograms with the straight and circular fringes are both symmetrical, for the straight fringes, we can get the same conclusion as the circular fringes. The larger the M, the smaller the RMS phase error is for APCA-LEF with different M. The RMS phase errors of GS and EVI are respectively 0.1423 rad and 0.1428 rad which are larger than that of APCA-LEF with any M except M = 1. For the complex fringes, the conclusion is a little different from the circular and straight fringes. For APCA-LEF, when M is less than 13, the larger the M, the smaller the RMS phase error is. However, the RMS phase errors in the situation of M = 21 and M = 25 are larger than that of M = 5, M = 9 and M = 13 since the interferograms with the complex fringes are asymmetrical, large M leads to the larger RMS phase error. The RMS phase errors of GS and EVI are respectively 0.2099 rad and 0.2509 rad which are larger than that of APCA-LEF with any M. Moreover, for both straight and complex fringes with 20 dB of noise, when M = 5, the RMS phase errors are both relatively smaller, so we can also choose 5 as the most appropriate value

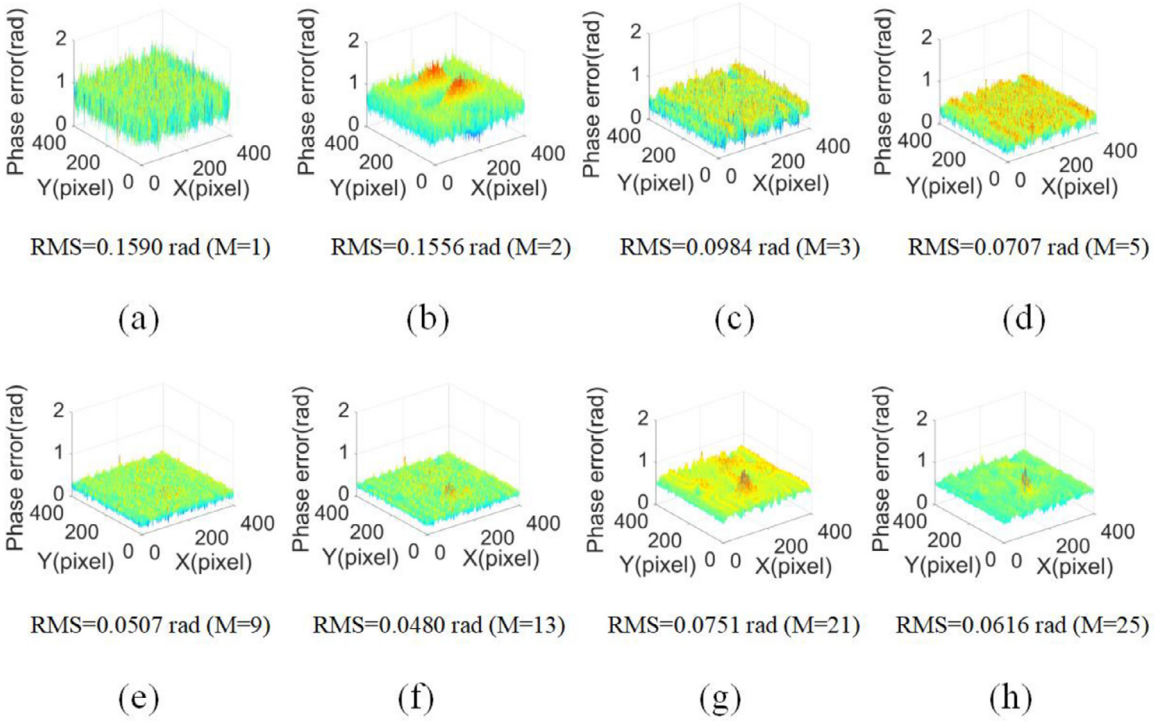

Fig. 13. The phase error distributions of the complex fringes using APCA-LEF with different M.

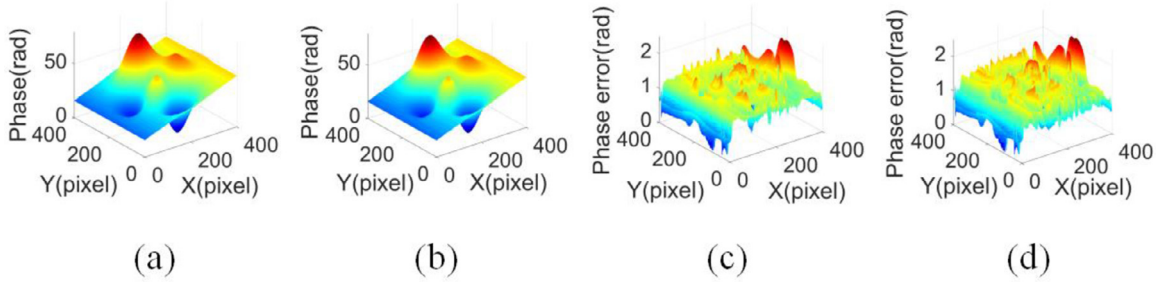

Fig. 14. Simulated results of the complex fringes using GS and EVI. (a) and (b) The phase distributions extracted by GS and EVI, (c) and (d) the phase error distributions of GS and EVI.

Table 1
Computational time of APCA-LEF with different M, GS and EVI.

	Time(s)	M = 1	M = 2	M = 3	M = 5	M = 9	M = 13	M = 21	M = 25	GS	EVI
Circular fringes	APCA	0.134	0.137	0.144	0.150	0.186	0.203	0.284	0.302	–	–
	LEF	0.900	0.902	0.918	0.899	0.901	0.915	0.912	0.923	–	–
	Total	1.034	1.039	1.062	1.049	1.087	1.118	1.196	1.225	3.032	3.071
Straight fringes	APCA	0.117	0.133	0.142	0.150	0.174	0.198	0.253	0.315	–	–
	LEF	0.901	0.905	0.899	0.869	0.881	0.890	0.887	0.880	–	–
	Total	1.018	1.038	1.041	1.019	1.055	1.088	1.140	1.195	2.446	2.385
Complex fringes	APCA	0.123	0.129	0.143	0.144	0.176	0.192	0.270	0.300	–	–
	LEF	0.892	0.903	0.892	0.872	0.905	0.896	0.882	0.905	–	–
	Total	1.015	1.032	1.035	1.016	1.081	1.088	1.152	1.205	2.434	2.390

of M for any kinds of fringes. Although the conclusion of the complex fringes is a little different from that of the circular and straight fringes, we can also get the conclusions that APCA-LEF, GS and EVI are all effective for the circular, straight and complex fringes, and APCA-LEF can get the higher accuracy with appropriate M than GS and EVI.

We also study the computational time of three different methods with different fringes, as shown in Table 1. Firstly, we study the computational time of APCA-LEF, we know that there are 2 steps for APCA-LEF, so we respectively calculate the computational time of every step with different M. Although LEF process costs more time than APCA process, it avoids the pre-filtering which will cost more time and decrease the accuracy. For APCA process, the larger the M, the more the computational time is. Moreover, LEF process is a fitting process, its computational time depends on not only the number of the pixels, but also the fitting difficulty. The less the noise, the easier the fitting process is, for the situation of M = 5, most of the noise is eliminated by the APCA process, so LEF process costs less time than any other situations. For the total time of APCA-LEF, the larger the M, the more the computational time is except M = 5, when M is larger than 9, the computational time is relatively long. Because the situation of M = 5 costs relatively less time

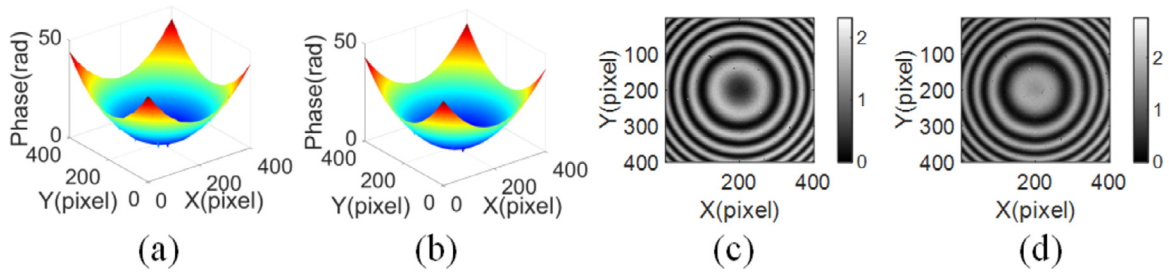

Fig. 15. Experimental phase distributions and two phase shifted interferograms. (a) The reference phase distribution extracted by 4-step PSA, (b) the phase distribution extracted by APCA-LEF in the situation of M = 1, (c) and (d) the first interferogram and the second interferogram.

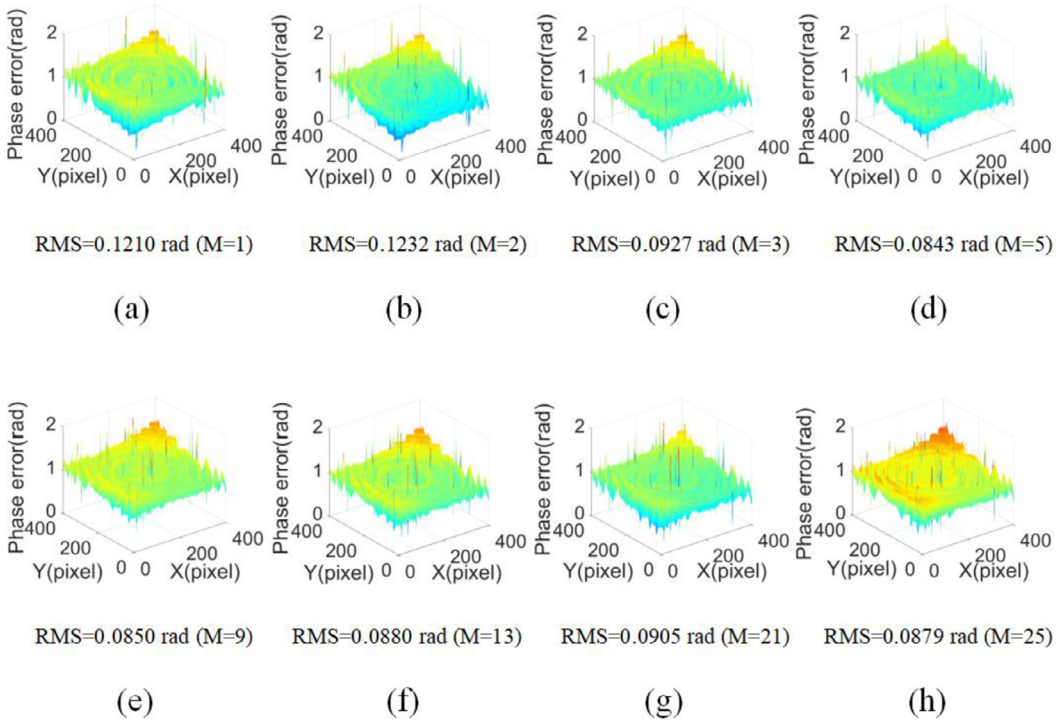

Fig. 16. The differences between the reference and phase distributions extracted by APCA-LEF with different M.

and obtain relatively higher accuracy, 5 is the most appropriate value of M. Lastly, we also compute the computational time of GS and EVI, they cost more time than APCA-LEF for any situation since the filtering process costs more time. From the above simulations, we can conclude that, APCA-LEF has more outstanding performance in regard to the different levels of noises, different phase shifts, different kinds of fringes and computational time than GS and EVI.

4. Experiment

To verify the performance of the proposed method, the experiment is performed to do the phase retrieval by the proposed method, GS and EVI. Four phase shifted interferograms with the circular fringes were extracted, and the phase shifts are respectively 0, $\pi/2$, π and $3\pi/2$, the size of interferograms is also 401 × 401 which is same as the simulation. Moreover, the phase extracted by standard 4-step PSA is set as the reference phase due to its high accuracy. Fig. 15(a) shows the reference phase distribution, and the phase distribution extracted by APCA-LEF in the situation of M = 1 is drawn in Fig. 15 (b), and the first two phase shifted interferograms are shown in Figs. 15(c) and (d). The differences between the reference and phase distributions extracted by APCA-LEF with different M are shown in Fig. 16. And we plot the curve of RMS phase errors with different M for APCA-LEF, as shown in Fig. 17. From

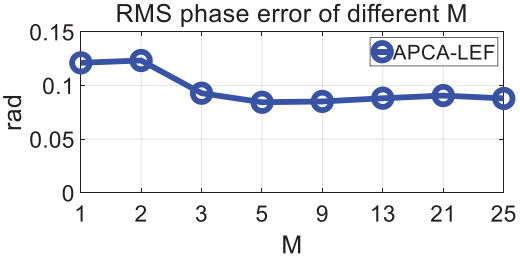

Fig. 17. RMS phase errors of different M for APCA-LEF.

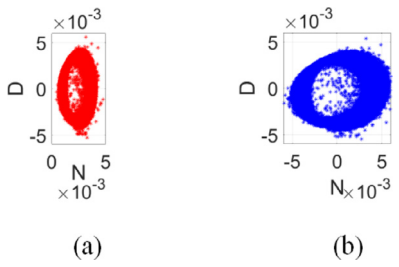

Fig. 18. The ellipses before and after using LEF for APCA-LEF in the situation of M = 1.

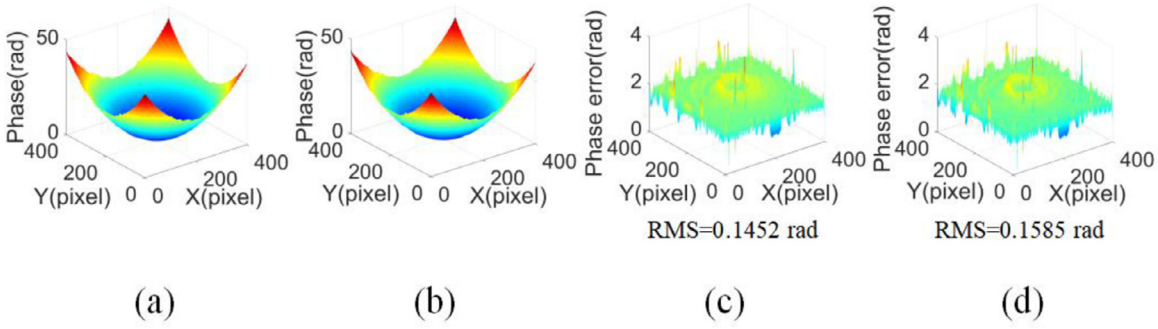

Fig. 19. The experimental results of GS and EVI . (a) and (b) The phase distribution extracted by GS and EVI, (c) and (d) the differences between the reference and phase distributions extracted by GS and EVI.

Table 2
Computational time of APCA-LEF with different M, GS and EVI.

Time(s)	M = 1	M = 2	M = 3	M = 5	M = 9	M = 13	M = 21	M = 25	GS	EVI
APCA	0.131	0.135	0.141	0.142	0.178	0.205	0.284	0.302	–	–
LEF	0.900	0.900	0.908	0.728	0.902	0.899	0.912	0.923	–	–
Total	1.031	1.035	1.049	0.87	1.08	1.104	1.196	1.225	2.868	2.926

Figs. 16 and 17, we can conclude that, the RMS phase error in the situation of M = 2 is largest since the effect of tilt error is larger than that of the systematic error, moreover, the RMS phase error in the situation of M = 5 is least. When M is between 1 and 5, the larger the M, the less the RMS phase error is except for M = 2, however, when M is between 5 and 25, the RMS phase error is increasing with the increase of M except M = 25. The experiment is similar to the simulation with the SNR of 40 dB except M = 25, the conclusion is not absolutely same to the simulation because the practical situation including the noise distribution, the background intensity and modulation amplitude distribution may more complex. The ellipses before and after using LEF are plotted in Fig. 18. Fig. 19(a) and (b) plot the phase distributions extracted by GS and EVI, and the differences between the reference and phase distributions extracted by GS and EVI are shown in Fig. 19(c) and (d). We can see that, the RMS phase errors of GS and EVI are similar and larger than that of APCA-LEF with any M.

Further, we study the computational time of APCA-LEF, GS and EVI, as shown in Table 2. We can get the same conclusion as the simulation, for APCA process, the larger the M, the more the computational time is, but for LEF process, the situation of M = 5 costs the least time. For the total time, the larger the M, the more the computational time is except M = 5, the situation of M = 5 costs less time than all other situations. Moreover, GS and EVI cost more time than APCA-LEF with any M. Hence, we can say that, when M = 5, APCA-LEF can obtain the high accuracy and cost less time simultaneously, 5 can be chosen as the most appropriate value of M.

After the simulation and experiment, we verify that, the proposed APCA-LEF without pre-filtering can obtain relatively accurate result with less computational time by only two interferograms.

5. Conclusion

In this paper, we present a PSA based on advanced principal component analysis and Lissajous ellipse fitting. APCA doesn't need to substract or filter the mean-background intensity, the adjacent pixels are taken part in the APCA process to increase the accuracy, and the LEF process is performed after APCA process to extract the real phase distribution. We have compared APCA-LEF with well-evaluated GS and EVI by the simulated and experimental data. The proposed method can extract highly accurate phase with less computational time. It removes the restriction that PCA needs more than three interferograms, it only needs two randomly phase shifted interferograms. Moreover, if the higher accuracy is requested, it's best to choose a phase shift which is far away from 0 rad and π rad. Lastly, 5 is the most appropriate value of M in regard to different levels of noises and computational time. The simulations and experiments demonstrate the validity of the proposed method. In summary, this proposed method is a power tool for the phase extraction with random phase shift.

Funding

This work was supported by the National Natural Science Foundation of China (NSFC) (61905039); Jilin Scientific and Technological Development Program (20190701018GH); Education Department of Jilin Province (JJKH20190691KJ) and State Key Laboratory of Applied Optics.

CRediT authorship contribution statement

Yu Zhang: Conceptualization, Methodology, Formal analysis, Writing - original draft, Funding acquisition. **Xiaobo Tian:** Investigation, Data curation, Software. **Rongguang Liang:** Writing - review & editing.

References

[1] Malacara D. Optical shop testing. 3rd ed. John Wiley & Sons, Inc; 2007. Chap 1-7.
[2] Bruning JH, Herriott DR, Gallagher JE, Rosenfeld DP, White AD, Brangaccio DJ. Digital wavefront measuring interferometer for testing optical surfaces and lenses. Appl Opt 1974;13(11) 2693–0703. doi:10.1364/AO.13.002693.
[3] Tian C, Liu S. Two-frame phase-shifting interferometry for testing optical surfaces. Opt Express 2016;24(16):18695–708. doi:10.1364/OE.24.018695.
[4] Malacara D. Optical shop testing. 3rd ed. John Wiley & Sons, Inc; 2007. Chap 14.
[5] de Groot PJ. Vibration in phase-shifting interferometry. J Opt Soc Am A 1995;12(2):354–65. doi:10.1364/JOSAA.12.000354.
[6] Deck LL. Suppressing phase errors from vibration in phase-shifting interferometry. Appl Opt 2009;48(20):3948–60. doi:10.1364/AO.48.003948.
[7] Wang Z. Advanced iterative algorithm for phase extraction of randomly phase-shifted interferograms. Opt Lett 2004;29(14):1671–3. doi:10.1364/OL.29.001671.
[8] Xu J, Xu Q, Chai L. Iterative algorithm for phase extraction from interferograms with random and spatially nonuniform phase shifts. Appl Opt 2008;47(3):480–5. doi:10.1364/AO.47.000480.
[9] Chen Y, Lin P, Lee C, Liang C. Iterative phase-shifting algorithm immune to random phase shifts and tilts. Appl Opt 2013;52(14):3381–6. doi:10.1364/AO.52.003381.
[10] Farrell CT, Player MA. Phase step measurement and variable step algorithms in phase-shifting interferometry. Meas Sci Technol 1992;3:953–8. doi:10.1088/0957-0233/3/10/003.
[11] Liu F, Wang J, Wu Y, Wu F, Trusiak M, Patorski K, Wan Y, Chen Q, Hou X. Simultaneous extraction of phase and phase shift from two interferograms using Lissajous figure and ellipse fitting technology with Hilbert-Huang prefiltering. J Optics-UK 2016;18:105604. doi:10.1088/2040-8978/18/10/105604.

[12] Vargas J, Quiroga J, Belenguer T. Phase-shifting interferometry based on principal component analysis. Opt Lett 2011;36(8):1326–8. doi:10.1364/OL.36.001326.
[13] Vargas J, Quiroga J, Belenguer T. Analysis of the principle component algorithm in phase-shifting interferometry. Opt Lett 2011;36(12):2215–17. doi:10.1364/OL.36.002215.
[14] Deng J, Wang K, Wu D, Lv X, Li C, Hao J, Qin J, Chen W. Advanced principal component analysis method for phase reconstruction. Opt Express 2015;23(9):12222–31. doi:10.1364/OE.23.012222.
[15] Xu J, Jin W, Chai L, Xu Q. Phase extraction from randomly phase-shifted interferograms by combining principal component analysis and least squares method. Opt Express 2011;19(21):20483–92. doi:10.1364/OE.19.020483.
[16] Yatabe K, Ishikawa K, Oikawa Y. Hyper ellipse fitting in subspace method for phase-shifting interferometry: Practical implementation with automatic pixel selection. Opt Express 2017;25(23):29401–16. doi:10.1364/OE.25.029401.
[17] Vargas J, Quiroga J, Sorzano C, Estrada J, Carazo J. Two-step demodulation based on the Gram-Schmidt orthonormalization method. Opt Lett 2012;37(3):443–5. doi:10.1364/OL.37.000443.
[18] Deng J, Wang H, Zhang F, Zhang D, Zhong L, Lu X. Two-step phase demodulation algorithm based on the extreme value of interference. Opt Lett 2012;37(22):4669–71. doi:10.1364/ol.37.004669.
[19] Luo C, Zhong L, Sun P, Wang H, Tian J, Lu X. Two-step demodulation algorithm based on the orthogonality of diamond diagonal vectors. Appl Phys B 2015;119:387–91 10.1007/s00340-015-6087-z..
[20] Niu W, Zhong L, Sun P, Zhang W, Lu X. Two-step phase retrieval algorithm based on the quotient of inner products of phase-shifting interferograms. J Opt 2015;17:085703. doi:10.1088/2040-8978/17/8/085703.
[21] Cheng Z, Liu D. Fast and accurate wavefront reconstruction in two-frame phase-shifting interferometry with unknown phase step. Opt Lett 2018;43(13):3033–6. doi:10.1364/ol.43.003033.